A novel setup for 3D chasing behavior analysis in free flying flies

Léandre Varennes, Holger Krapp, Stéphane Viollet

A novel setup for 3D chasing behavior analysis in free flying flies

Léandre Varennes, Holger Krapp, Stéphane Viollet

A novel setup for 3D chasing behavior analysis in free flying flies

Léandre P. Varennes[a,b,*], Holger G. Krapp[a], Stéphane Viollet[b]

[a] Department of Bioengineering, Imperial College London, SW7 2AZ London, UK
[b] Aix-Marseille Universite, CNRS, Institute of Movement Science, UMR 7287, Marseille 13288, France

ARTICLE INFO

Keywords:
Aerial pursuit
Free flight
Blowfly
Invertebrate pursuit
Capture strategies
Insect vision
Neuroethology
Fly body orientation

ABSTRACT

Background: Insects catching prey or mates on the wing perform one of the fastest behaviours observed in nature. Some dipteran flies are aerial acrobats specialized to detect, chase and capture their targets within the blink of an eye. Studies of aerial pursuits and its underlying sensorimotor control have been a long-standing subject of interest in neuroethology research.

New method: We designed an actuated dummy target to trigger chasing flights in male blowflies. Our setup generates arbitrary 2D target trajectories in the horizontal plane combining translation up to 1 m/s and angular rotation up to 720°/s.

Results: Using stereovision methods we reconstructed target and pursuer positions every 5 ms with a maximum 3D error of 5 mm. The pursuer's body pitch and yaw angles were resolved within an error range of 6deg. An embedded observation point provides a close-up view of the pursuer's final approach and enables us to measure its body roll angle. We observed banked turns and sideslip which have not been reported for chasing blowflies in the past.

Comparison with existing method(s): Previous studies focused on pursuit along circular paths or interception of translating targets while our method allows us to generate more complex target trajectories. Measurements of body orientation in earlier accounts were limited to the heading direction while we extended the analysis to include the full body orientation during pursuit.

Conclusions: Our setup offers an opportunity to investigate kinematics and governing visual parameters of chasing behaviour in species up to the size of blowflies under a large variety of experimental conditions.

1. Introduction

Flying insects are one of the most manoeuvrable animals on the planet. We often take the example of flies escaping from an attempt to swat them as a demonstration of their fast reactions, but their airborne chasing behaviour is even more impressive. Taking advantage of its exceptional manoeuvrability, the chasing fly is capable to deal with unpredictable trajectory changes and evasive tactics of its target while avoiding obstacles. Fly sensory-motor responses to correct their trajectories kick in only about 20 ms after course changes of its target (Collett and Land, 1975) as a result of neuronal processing delays and the time it takes steering motor action to become effective. Previous studies have been aiming to observe and understand the complexity of chasing flights and its underlying control at different systems levels (Egelhaaf and Borst, 1993).

Chasing has been characterized under natural free flight condition in various species: the housefly *Musca* (Wehrhahn, 1979; Wehrhahn et al., 1982; Wagner, 1986a), its smaller relative *Fannia* (Land and Collett, 1974), patrolling males (Zeil, 1986), the hoverflies *Syritta* (Collett and Land, 1975), *Eristalis* and *Volucelle* (Collett and Land, 1978), and dilochopodid flies (Land, 1993). Similar types of experiments were performed on dragonflies capturing *Drosophila* (Olberg et al., 2000; Mischiati et al., 2015).

In the late 1970s, Collett and Land observed that hoverflies pursued a cherry core after one of them spit one near a bush, inspiring the scientists to build a pea-gun for studying the flies' pursuit reflex (Collett and Land, 1978). Much later in early 2000s, to elicit prey capture Olberg et al. (2007) attached a bead to a fishing line and moved it by hand in the same plane as a perching dragonfly. In a recent study on dragonfly pursuit, Mischiati et al. (2015) also used a bead fixed on a transparent fishing line. This time the bead moved in straight line, at a computer-controlled speed, with height-adjustable pulley system. A similar study has been performed with robberflies by Wardill et al. (2017) and a much smaller aerial predator, the killer fly (Wardill et al.,

* Corresponding author at: Institut des Sciences du Mouvement, Bât soufflerie - CP 910, 163 avenue de luminy, 13009 Marseille, France.
E-mail addresses: l.varennes-phillit14@imperial.ac.uk, leandre.varennes-phillit@univ-amu.fr (L.P. Varennes), h.g.krapp@imperial.ac.uk (H.G. Krapp), stephane.viollet@univ-amu.fr (S. Viollet).

https://doi.org/10.1016/j.jneumeth.2019.04.006

2015). To summarize, targets triggering interception behavior were moved by hand, shot at a close proximity of pursuers or moved at various speeds along straight trajectories.

Boeddeker et al. (2003) reported the first study on chasing behavior where the speed of a dummy target was controlled more systematically. Male blowflies were pursuing a black sphere (dummy) moving at constant speed along a circular path of 10 cm radius. In a series of experiments, the speed (1/1.25/1.5 m/s) and the size (5/8/13 mm) of the target were varied, revealing the parameter combination required for male flies to capturing the dummy. The scientists also provided a model describing the dynamics of the male blowfly's chasing flights in the horizontal plane. However, despite the excellent repeatability of the behaviour, the comparatively regular dummy trajectories used in those experiments are quite different from the complex trajectories observed under more realistic conditions. To overcome these limitations, we developed a method that enables us to study chasing behaviour in male flies confronted with target trajectories which more closely approximate the female flight dynamics. Here we describe (i) the system that controls target motion, including its mechatronics, (ii) a high speed camera-based 3D tracker based on which dummy and fly trajectories are reconstructed, as well as the orientation of the pursuer (yaw- and pitch-) and (iii) preliminary experimental results obtained with the blowfly *Lucilia sericata*. The setup can be upgraded with a novel observation system that provides high quality imagery of the pursuer's final approach offering valuable details of the capture phase, and measure of the body roll.

2. System description

2.1. Principle of operation

The custom-made flight arena is a rectangular volume of 70 × 50 × 50 cm. Flies have a spectral sensitivity slightly shifted to lower wavelengths compare with humans, excluding the red color spectrum above 650 nm (Menzel and Backhaus, 1991; Harris et al., 1976). Thus we covered the walls with a 1D visual grating consisting of vertically oriented red and white stripes (Figs. 1A and 2). Similar patterns have been used previously in experiments on honeybees passing through a long tunnel (Portelli et al., 2010). They are creating visual information, needed by the flying insects to stabilize their flights. In our setup, the objectives of the two cameras were equipped with optical red filters to minimize the contrast between the red and white stripes so the background appears close to a uniform intensity distribution in the video footage. On top of the arena, we implemented an actuated pulley system controlling the movement of the target.

2.1.1. Moving the target

To accurately generate complex target trajectories, we implemented a 2D positioning system called CoreXY (see Fig. 1B) developed by Mayer (2012), which is an upgrade of the H-frame XY positioning system (Sollmann et al., 2010). Those activated systems are widely used to position a part or a tool within a 2D area, often used in 3D printers. The smooth and fully controlled trajectories the CoreXY system generates when mounted on top of the arena (see Fig. 1A) are close to the dynamics of chasing flights.

The mechanical assembly adapted from an H-frame positioning system enables high acceleration and therefore faster movement control than the traditional H-frame system. In our positioning system, there are two parallel tracks (linear extruded rails) along which another couple of rails called bridge can slide by using pulleys mounted like dolly wheels (see Fig. 1B). The cart slides on the bridge by using the same principle based on dolly wheels. At each end the two parallel tracks sits on a pulley. The ones at the lower end are directly connected to the motor shafts of stepper motors which drive the toothed belt controlling the movements of the positioning system. The CoreXY system features two differences from an H-frame. Together these differences result in the major advantage regarding the power required to move the cart carrying a given amount of payload (see below). First, an extra couple of pulleys change the belt circuit, enabling the belt to cross outside of the working range (see Fig. 1B). The second difference concerns the 4 attachment points establishing the link between the belt and the cart as opposed to only two in the H-frame design. Distributing the effort equally over 4 attachment points means that we can move an heavier payload on the cart for the same amount of power generated by the motors. The ceiling of the flight arena is made of white fabric that slides gently over the main structure when the cart moves, which prevents flies to escape during experiments. The moving cart in Fig. 1C supporting the rotating target is composed of two co-axial shafts: (i) a fixed inner shaft (diameter 6 mm) containing the light guide of an embedded camera and preventing connected wires to twist, as well as (ii) a rotating outer shaft to which a rod holding the target and, at the end, a tilted mirror are attached.

The outer shaft (in red in Fig. 1C) is actuated, through a belt, by a small stepper motor (Faulhaber, AM0820-V5-56, reduction gear ratio of 1). The latter is controlled at a resolution of 1200 steps per revolution allowing for a maximum rotational speed of 720°/s.

Target movements are thus controlled along the two translational degrees of freedom in the horizontal plane by the CoreXY system and one rotational degree of freedom by the mounted stepper motor. The CoreXY system alone reaches translations of up to 1 m/s, which can be combined with maximum angular velocities of two revolutions per second, enabling large variety of target movements. The target is placed 15 cm below the ceiling and can reach any position within the floorplan of the arena.

Translation: In the following we give the equations of motion the CoreXY generates. The two actuators are the two stepper motors A and B and the moving object is the cart (see Fig. 1B). Activating only one motor while keeping the other one still results in linear motion of the cart. Positive rotation (counter clockwise) of motor A while holding motor B still results in diagonal cart movement in the positive x- and positive y- direction, while a negative rotation of the same motor causes a movement in negative x- and negative y-direction. This can be written as:

$$\Delta A = \Delta X + \Delta Y \tag{1}$$

Activation of motor B, while keeping motor A stationary, moves the cart along the other diagonal. In this case positive rotation of motor B results in a movement of the cart in positive x- and negative y-direction.

$$\Delta B = \Delta X - \Delta Y \tag{2}$$

Combining Eqs. (1) and (2), we obtain the movement of the cart along the x- and y-axis as a function of activation of motors A and B:

$$\begin{cases} \Delta X = 1/2(\Delta A + \Delta B) \\ \Delta Y = 1/2(\Delta A - \Delta B) \end{cases} \tag{3}$$

We can describe the general relationship between the rotation of the motor pulley and the displacement of the belt moving the cart by:

$$\Delta M = r\Delta\phi_M \tag{4}$$

Where r the radius of the motor pulley, $\Delta\phi_M$ is the number of angular steps (in radians) in the ϕ_M direction, and ΔM is the displacement of the belt. Thus, by substituting the activity of motors A and B in Eqs. (3) and (4) we obtain the movement of the cart along x- and y-axis as a function of the rotation of motors A and B.

$$\begin{cases} \Delta X = \mathrm{rR}/2(\Delta\phi_A + \Delta\phi_B) \\ \Delta Y = \mathrm{rR}/2(\Delta\phi_A - \Delta\phi_B) \end{cases} \tag{5}$$

We used a GT 5 mm timing belt mounted on step motors pulleys of 30 teeth. By adding micro-step drivers (with reduction ratio R), we can increase in precision the displacement of the cart. In our system $r = 23.85$ mm and $R = 1/4$.

Rotation: The rotation of the target around the center of the cart is

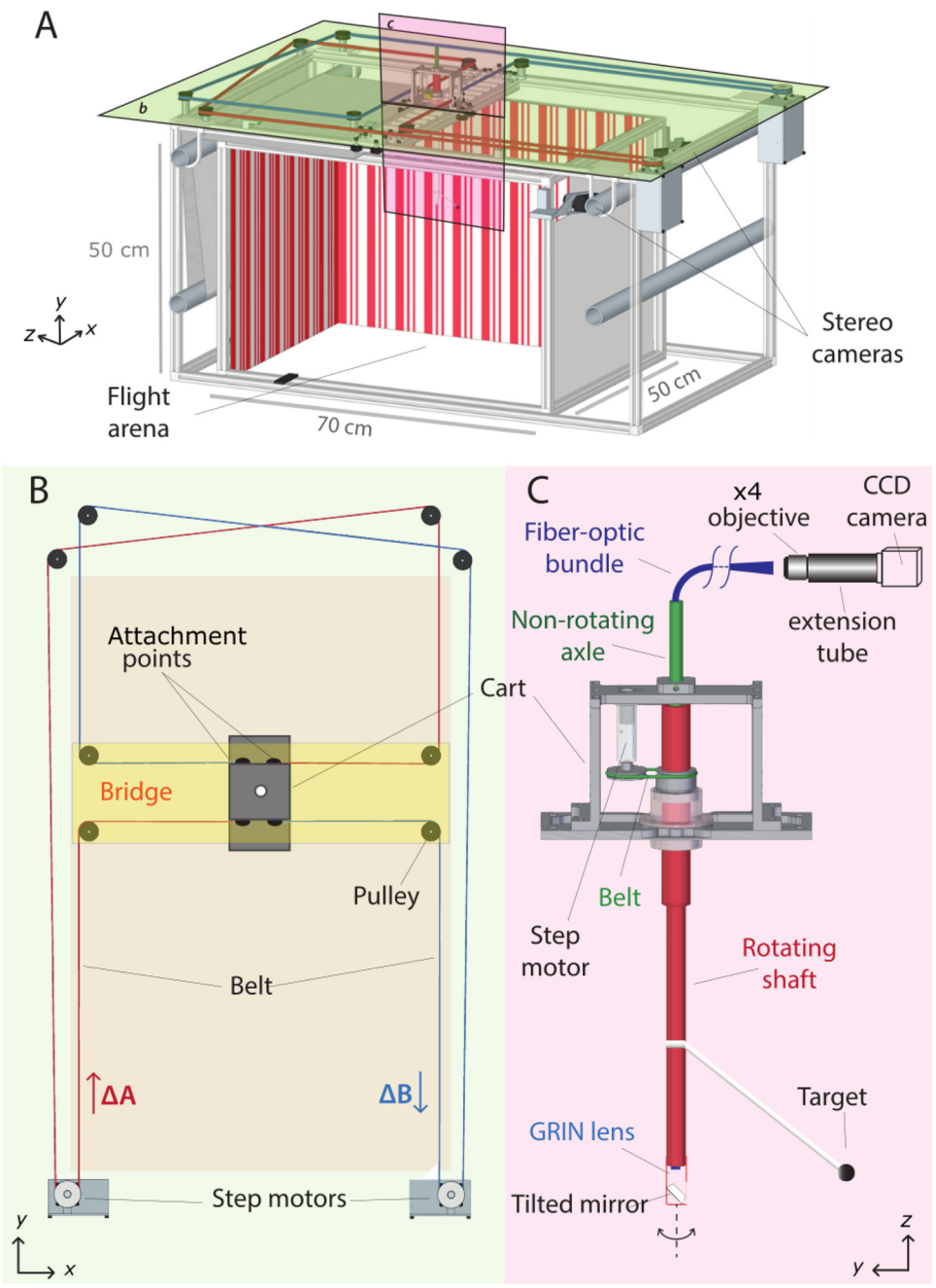

Fig. 1. Schematic view of the chasing arena. (A) Global view of the setup. (B) Top view of the setup presenting the CoreXY technique adapted from (Mayer, 2012). The moving platform or cart (gray central rectangle) translates along the *x*-axis inside the yellow zone called bridge. The bridge moves along the *y*-axis. By controlling simultaneously the two translations, the cart can move within its working range shown by the pale orange zone. (C) Side view of the cart equipped with a stepper motor that rotates the belt and thus the rotating shaft supporting the target. Other components are parts of an embedded micro-endoscope described in details in Section 4. For the sake of clarity, the rotating and non rotating shafts are coloured (in red and green) on the schematics, but are white in the actual setup.

presented as follow:

$$\theta(t + \mathrm{dt}) = \theta(t) + \Delta\phi_{\mathrm{CAM}}\cdot\mathrm{res}\cdot\mathrm{dt} \tag{6}$$

with θ the angular position of the target with respect to the cart frame, dt the time between two commands (10 ms), $\Delta\phi_{CAM}$ the number of angular steps (in radians) in the ϕ_{CAM} direction and res = 2π/1200 in steps per revolution.

Finally, the position of the target (ΔX_{Tar}, ΔY_{Tar}) is a combination of the CoreXY control of the cart (ΔX, ΔY) and the control of the rotation by the embedded system. It can be written as:

$$\begin{cases} \Delta X_{\mathrm{Tar}} = \Delta X - \cos(\theta)\cdot l \\ \Delta Y_{\mathrm{Tar}} = \Delta Y - \sin(\theta)\cdot l \end{cases} \tag{7}$$

with l = distance(Mirror − Target) in millimetre.

Considering target movement at 1 m/s along the first diagonal we described above (positive *x* and *y*-axis movement) at 1 m/s, all movement would be caused by motor *A*: $\Delta X = \Delta Y$ then $\Delta B = 0$. With a pulley radius, *r* of 23.85 mm a maximum angular rotation of 41.93 rad/s or 6.52 rev/s (see Eq.(4)) results, which is within the normal working range of the stepper motors.

2.1.2. Videography, object tracking and image analysis

We implemented two CCD cameras CAM1 and CAM2 (PROSILICA GC640, spatial resolution of 640 × 480 pixels, temporal resolution of 200 frames per second), equipped with optics used at fixed focal depth (6 mm, $F = 1.4$). Those synchronized cameras were arranged to set up a stereovision system that records the chasing sequences.

We used an open access tool (DLTdv5) which offers efficient calibration, tracking and 3D reconstruction capabilities (Hedrick, 2008) using the Direct Linear Transformation (DLT) technique described by Aziz and Karara (1971). We followed the DLTdv5 calibration procedure applied to a custom built calibration cube with an edge length of 30 cm, the 64 individual markers spaced at 100 mm distances from each other

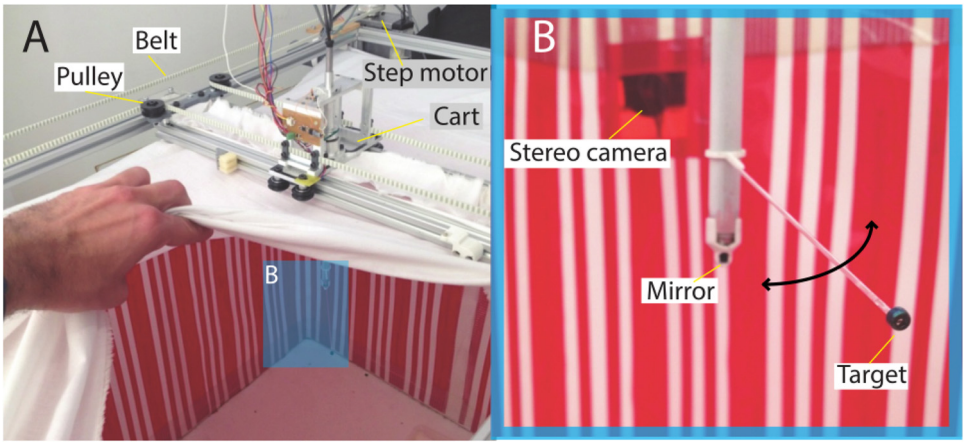

Fig. 2. Chasing arena. Picture of the chasing arena from outside (A) and from inside (B) with a close-up view on the target placed at the tip of a rod that is attached to an actuated rotating shaft. The latter supports both the rod and the small mirror enabling them to rotate simultaneously.

along all three dimensions. Then, we created a file containing the absolute position of each individual marker, and we determine their position in the two corresponding image frames obtained by CAM1 and CAM2. The toolbox generated a file (csv format) containing the 11 DLT coefficients, specific for our stereovision system, describing positions of the cameras and their orientation relative to each other (for more details see Hedrick, 2008).

The DLTdv5 toolbox includes an integrated tracker module that computes the trajectories of multiple objects in a sequence of stereo images. In our case we track two objects: the target and the chasing fly. The tracker can be applied in different modes (automatic, semi-automatic, and manually) and runs a predictive algorithm based on Kalman-filtering to overcome missing matches of the tracked object due to temporary occlusions or excessive object accelerations. As shown in Fig. 6 we successfully used the DLT method to reconstruct the centre of mass of the target and the fly in 3D based on consecutively tracked points. The fly's centre of mass identified in the previous image frame of the sequences (2D) defines the Region Of Interest (ROI) for the subsequent tracking step. The application of an in-built 2D zoom to each frame allows us to identify and label the fly's head and abdomen to retrieve the animal's 3D body orientation. We validated the method by comparing the computed distance between the head and tip of the abdomen with the actual length of the fly.

2.2. Accuracy of generating and reconstructing target trajectories

To assess the accuracy of generating target movements and their 3D reconstructions using the CoreXY system, we studied the positioning error of a circular and an ellipsoid trajectory across eleven trials each. Both trajectories covered a large section in the horizontal plane of the experimental arena (Figs. 3A and 4 A). First, an initialization phase brought the cart to a reference point close to one of the walls defined by electromagnetic stops. Then the cart moved away from the wall and reached its cruising speed. The desired trajectory can start, here three successive circles on each of the 11 tries. The mirror and target positions were measured every 10 ms, where the mirror is considered to be placed in the centre of the cart. For the circular trajectory, we obtained standard deviations (SD) of the mirror position along the x, y and z axes as small as 2.07, 3.34 and 0.76 mm, respectively (Fig. 3C), and SD = 4.23, 5.65 and 0.97 mm along the three axes for the target position. During this circular trajectory, the mirror and the target travelled 1.7 and 2.5 m, respectively. On the ellipsoid trajectory the mirror is still moving on a circular path, but the target generates an elliptical movement along which it changes its velocity profile. The standard deviations based on data across 11 trails were even smaller than those for the circular trajectory. The highest SD (for the y-axis) was below 3 mm for the mirror and below 4 mm for the target (Fig. 4).

2.3. Spatial resolution of the cameras

The spatial resolution of any object in the recorded video footage depends on the pixel resolution the cameras used in relation to the distance-dependant size of the objects. CAM1 and CAM2 recorded images at a resolution of 640 × 480 pixel (see Section 2.1.2). The focus of the cameras was adjusted to the centre of the arena, about 50 cm away from the cameras. At this position 1 pixel on the cameras' CCD sensor corresponds to 0.73 × 0.97 mm along the spatial x- and y-dimension (assuming no image deformation). This means that the smallest silhouette of the fly with a diameter of 4 mm, i.e. when the fly is directly facing the camera (without considering wings or legs), will be mapped onto about 17 pixels of the CCD sensor. This number of pixel proved to be sufficient to extract the animal's body ellipse using custom-made image processing tools.

To assess the performance of the system we designed a test module that was attached to the cart of our experimental setup. It consisted of a rotating shaft to which a rod was attached at the end of which a dead specimen (male *Lucilia Sericata*) was suspended (Fig. 5A).

The longitudinal body axis of the specimen was aligned with the centre (optical axis) of a mirror implemented at the lower end of the shaft. The distance between the mirror and the specimen (**Ra**) was 45 mm. Compared to life male flies which measure about 10 mm along their longitudinal body axis, the dead specimen was smaller with a length of about 7.5 mm – probably due to desiccation. The rotating shaft holding the mirror was moved on a circular path (Fig. 5B black trajectory) while itself turning at 1000°/s. As a result, the dead specimen did temporarily move at higher speeds than described for the mirror and target of the CoreXY system in Section 1, more closely approximating natural chasing flights (Fig. 5C). These compound trajectory cover a large range of variations of fly and mirror orientations within a large part of the arena. The trajectories were recorded two times with both cameras at 190 frames per second (N = 1191 frames). We assessed the spatial resolution of our method by comparing the known distance between the mirror and the fly (45 mm) and the fly length (7.5 mm) with the values produced by the 3D reconstruction system. The a associated with $PT(\theta a, \varphi a, Ra)$ denotes the target bearing angle, or absolute line which connects the center of mass of the fly Q, and the center of mass of the target T. The b associated with $OP(\theta b, \varphi b, Rb)$ denotes the pursuer heading angle, or longitudinal body axis of the Pursuer (b for body), that connects the top of the head H to the tip of the abdomen O (see Fig. 5E). The system returned a mean fly-mirror distance **Ra** of 45 ± 5 mm SD and a mean fly length **Rb** of 7.5 ± 1 mm SD (see Fig. 5D).

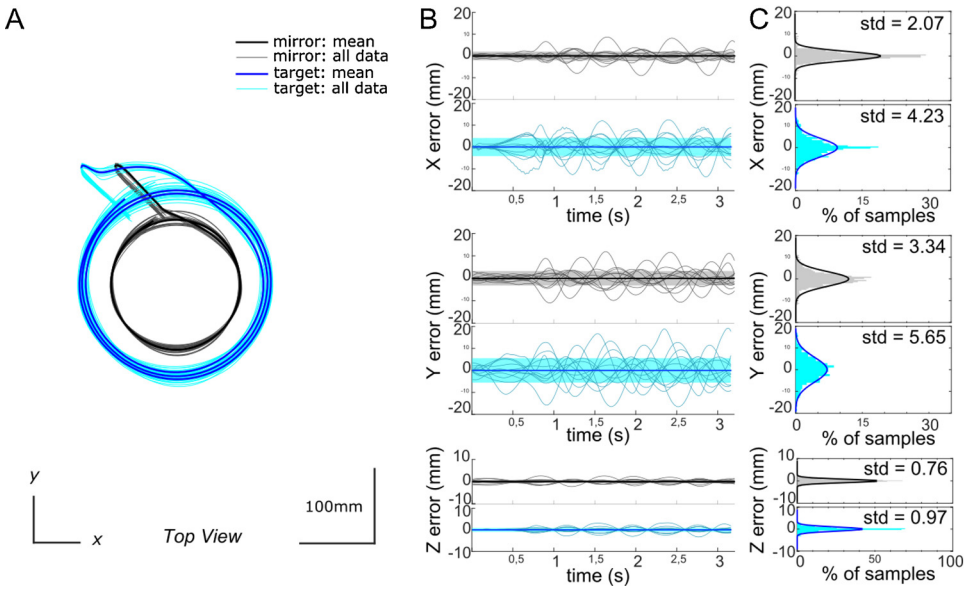

Fig. 3. Precision of a circular target trajectory across 11 trials. (A) Superimposed circular trajectories reconstructed by the calibrated stereo vision system. Successive loops do not overlap perfectly: this is partly due to mechanical imprecision in moving the target, and party due to imprecision in the video tracking. (B) Superimposed plots of the x-, y-, and z-components of the positional error observed for the target (blue) and the mirror (black) over time. The mirror positions are given in grey with the std window, and the target positions in blue graphs. (C): Distribution of errors + Gaussian fits for the mirror and the target positions along the x-, y- and z-axes. (std = standard deviation).

As the longitudinal body axis of the fly was aligned with the specimen-mirror line, we could determine the azimuth and elevation error angles between those two axes. We found a mean azimuth error of $-3 \pm 6^{\circ}$ SD and a mean elevation error of $-3 \pm 3^{\circ}$ SD. Making the hypothesis that the head and body are fixed, when reconstructing the field of view of the pursuer, those errors of body orientation will represent an error of a couple of ommatidia for *Lucilia Sericata*.

3. Analysing 3D chasing flights

We used the novel setup to record chasing flights in blowflies (*Lucilia Sericata*). Pupae were purchased from an animal supplier (BioFlyTech) in Spain. For further work, we have established a breeding. Male flies aged between 5 and 12 days were placed in the arena. They were exposed to a 12:12 h light:dark cycle with a luminance of about 2000 cd m^{-2} at a temperature between 20 and 25 °C. They stayed in the arena without engaging in an experiment for one day to get used to their new environment. Chasing flights were recorded around noon, during their peak activity phase. We used a black sphere of 8 mm diameter as a target.

3.1. Parameters describing strategies of catching targets

Animals have developed different strategies to catch prey or conspecifics. Even in flying insect species of similar size, depending on the specific task, the strategies may be as different as chasing or intercepting a given target (Pal, 2015; Gonzalez-Bellido et al., 2016). To distinguish between those strategies quantitatively requires the identification and characterization of relevant parameters that determine the given flight behavior. In this section we will describe some of the parameters our experimental setup allows us to capture. We recorded free fight pursuits at a rate of 190 fps, corresponding to a time resolution of 5.3 ms. The 2-dimensionally tracked positions of the target and the pursuer were computed with the DLT coefficients (on how to get those coefficients see Section 2.1.2 and Hedrick, 2008) to reconstruct their 3D positions. When presenting the flies with a circular target trajectory we observed essentially the same behaviour as Boeddeker et al. (2003), who distinguished between 'capture-' and 'pursuit-flights'. In the former case, the pursuing fly soon captures the target while in the latter case the animal pursues the target moving on a circular trajectory for at least one circle (about 650 ms with a target moving at 1 m/s).

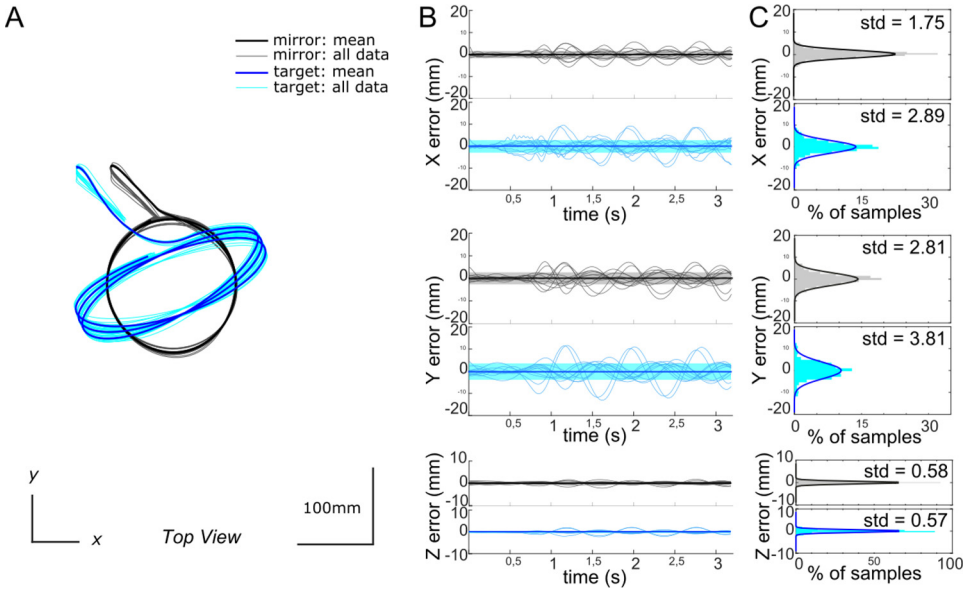

Fig. 4. Precision of a ellipsoidal target trajectory across 11 trials. (A) Superimposed circular trajectories reconstructed by the calibrated stereo vision system. (B) Superimposed plots of the x, y, and z components of the positional error observed for the target and the mirror over time. (C) Distribution of errors + Gaussian fits. See Fig. 3 for details.

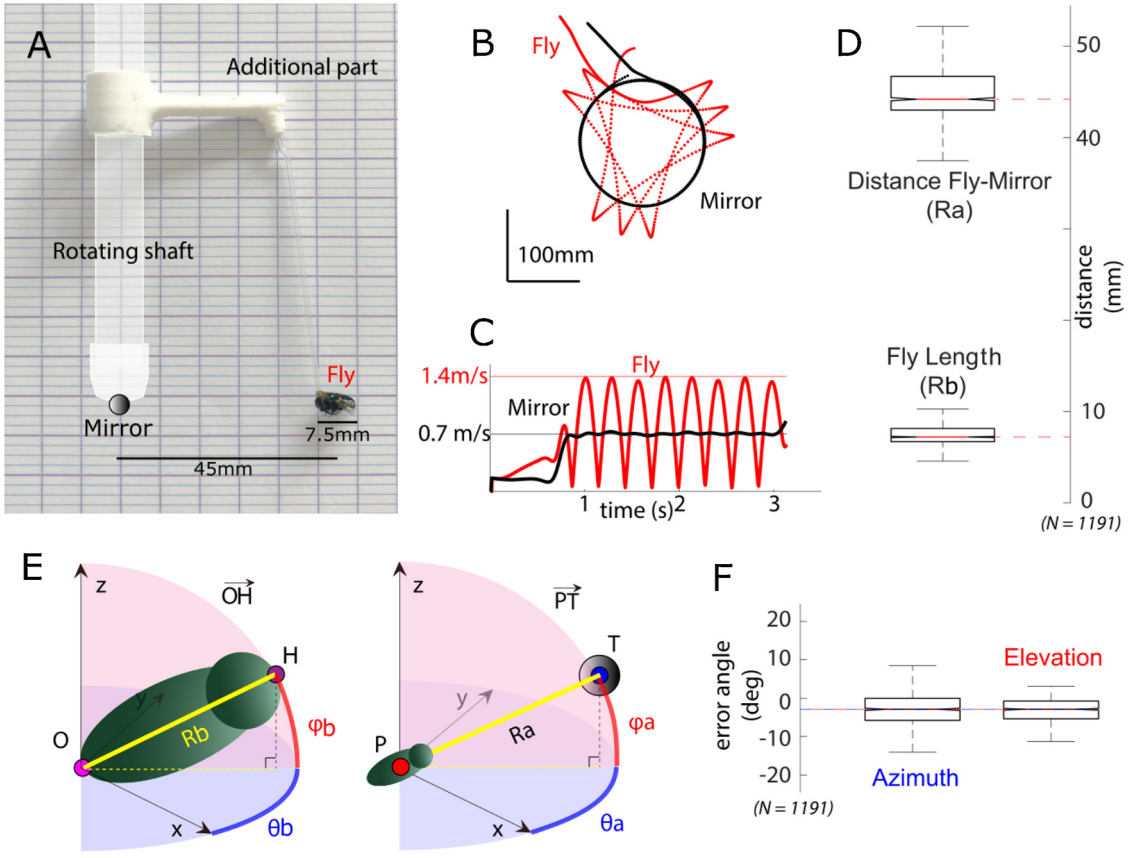

Fig. 5. Validation of the 3D trajectory reconstruction method. (A) A dead specimen was attached to a transparent off-axis rod and aligned with a mirror at a distance of 45 mm. The fly's length along its longitudinal body axis was about 7.5 mm. (B) top view of the measured trajectory of the mirror (black) and the specimen (red). Black scale bars refers to *x*- and *y*-axis of the arena. (C) Mirror and specimen velocities of the trajectories presented in (B) plotted as a function of time. The mirror moves at a constant speed of 0.7 m/s (black trace). The specimen is moved around the mirror with an angular velocity of almost 1000°/s and presents a linear velocity range between zero and 1.4 m/s (red trace). (D) Measured distances. *Top*: Distance Fly-Mirror, **Ra**: median = 44.18 mm; mean = 45.14 ± 5.26 mm SD. *Bottom*: Fly length **Rb**: median = 7.23 mm; mean = 7.53 ± 1.24 mm SD. (E) Tracked points of interest. *Left*: The line **OH** describes the specimen's orientation defined by the tip of the abdomen, **O**, and the front of the head **H**, given in spherical coordinates (θb, φb, *Rb*, b for body). *Right*: The line **PT**, connects the center of mass **P** of the specimen (P for pursuer) with the center of mass **T** of the target, in spherical coordinates *PT*(θa, φa, *Ra*). (F) Angular resolution. Errors were obtained by calculating the difference between the vectors **PT** and **OH** shown in (E) (comp A − comp B). *Left*: Azimuth error ($\theta a - \theta b$): median = −2.89°; mean = −3.07 ± 5.88°. Elevation error ($\varphi a - \varphi b$): median = −2.89°; mean = 3.32 ± 3.19°. Medians, means and SDs based on $N = 1191$ frames.

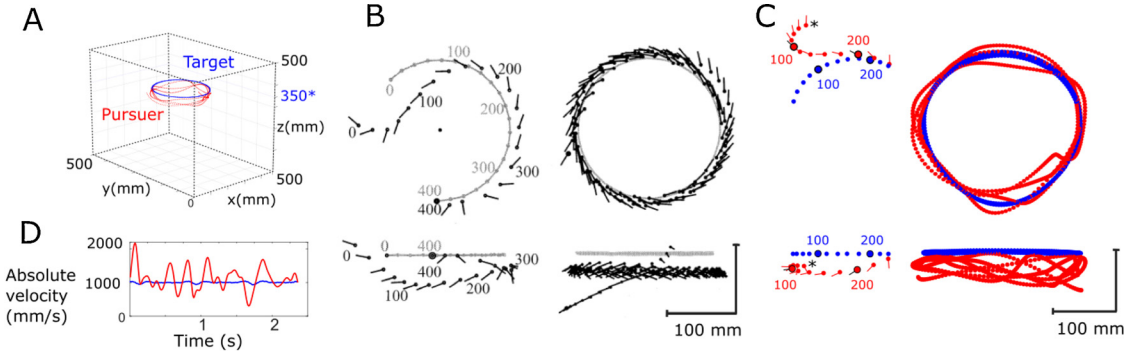

Fig. 6. Preliminary results: Example of fast capture and long pursuit characterization. (A) Reconstruction of a male blowfly chasing a dummy target. (B) *Left*: Reconstructed 3D trajectory of a fly (black markers) capturing the target (grey markers) viewed from on top and from the side. Filled circles and lines indicate the fly's centroid position and body orientation, respectively. The numbers denote time stamps during the chasing flight spaced at 100 ms. *Right*: Chasing flight without target capture. Results shown in *left* and *right* subplot copied from Boeddeker et al. 2003. (C) Pursuit of the target during a similar experiment as shown in (B), performed in our chasing arena. *Left*: Reconstruction of a fly (red markers) capturing the target (blue markers) during a fast capture (250 ms). For sake of clarity the positions are placed every 20 ms, and except for colors, the caption is the same as in (B). *Right*: Reconstruction of a long pursuit without target capture (data from subfigure A). Each dot indicates the centre of mass of the target (blue) and the fly (red) plotted every 5 ms. For sake of clarity the body orientation and time stamps are not presented here. (D) Absolute velocity of the target and the fly during pursuit seen in subfigure (A and C, *Right*). The target speed is centred around 1 m/s whereas the pursuer's speed reached peak values of up to 2 m/s.

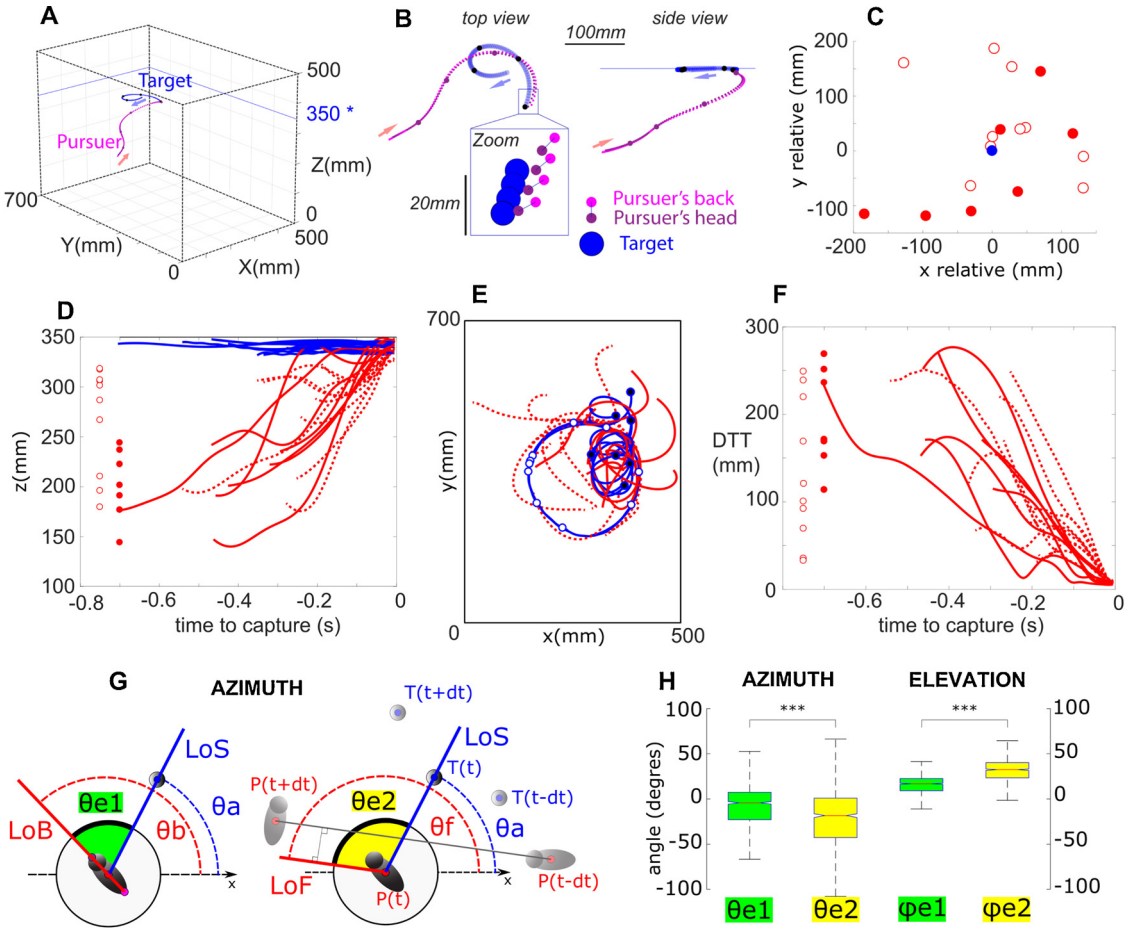

Fig. 7. Preliminary results: Analysis of dynamics in a capture. (A) Reconstruction of a chasing flight after a target moving along a 'spinning top trajectory'. Bigger points mark positions reached after 100 ms time intervals. The target is moving in the horizontal plane indicated by the blue lines (350*). Arrows show the direction of the target and the pursuer at the beginning of the sequence. (B) Top and side view of the chasing flight shown in (A). Head and tip of the abdomen of the pursuer are represented by differently coloured markers. The high degree of overlap of the markers demonstrates the robustness of the method. (C) Relative position of the pursuer when initiating the pursuit (top view). Two types of target trajectories are presented: open circles for the 10 circular trajectories, and filled circles for the 8 spinning top trajectories (target in blue). (D) Altitude change of the pursuer before target capture. Dots on the left give the detection altitude (mm) of the pursuer for each chase. (E) Top view of the chases. Note the distinct target trajectories, Central Circle, and Spinning Top on the right side of the circles. Positions where the fly initiates the pursuit are shown in white filled dots for Circle Trajectories, and black filled dots for spinning top trajectories. The black rectangle represents the experimental surface. (F) Change of the Distance To Target (DTT) before the capture. Dots represent the detection DTT of each pursuit. Opened markers for circular trajectories, and filled markers for spinning trajectories. (G) Definition of the measured angles. From the top view only the azimuth component of the error angles is available. *Left*: The error angle $\theta e1$ or Target Heading angle is defined by the angle made between the Line of Sight (LoS azimuth: θa, or target bearing angle) and the longitudinal body axis (LoB for Line of Body, azimuth: θb, also Yaw of the fly). *Right*: Part of a pursuit sequence. Three consecutive horizontal positions of the Target (T) and of the Pursuer (P) are represented by their center of mass. The Line of Flight of the pursuer at time t is the line joining previous and next positions (LoF azimuth: θf). This line plotted on the point P(t) is similar to the tangent of the trajectory on this point. The Error angle $\theta e2$ describes the Target relative bearing. It is the angle made by the Line of Flight of the pursuer and the Line of Sight. (H) Boxplot of the two components (azimuth θ and elevation φ) of the two error angles for the 17 captures presented above. These two error angles are significantly different on both planes (Ttest, p(az) = 9E-17, p(el) = 2E-100, see ***, $N = 1104$).

Examples of both flight type trajectories reported by Boeddeker et al. (2003) are shown in Fig. 6B. For comparison Fig. 6C shows similar flight trajectories studied with our novel setup. In both pursuits the fly chases the target moving along a circular path at a constant speed of 1 m/s. The absolute velocity profiles of the target and the long pursuit flight are shown in Fig. 6D, where we can see that the fly velocity varies a lot, and it reaches a maximum of 2 m/s. The 3D reconstruction of the sequences provides valuable information about the fly's strategy to capture the target. In both types of chasing flights (fast capture or long pursuit see Fig. 6C), the flight path of the fly suggests that it is not guided by an interception strategy. Instead, the fly closely follows the circular trajectory of the target. To investigate the behaviour in more detail we presented our flies with more complex target trajectories.

Fig. 7 shows a fast capture when the target follows a type of trajectory different from a circle. We called this specific trajectory the 'spinning top'. It consists of a simple translation along the *y*-axis combined with a rotation of the target around the *z*-axis. The rod, the target is attached to, rotates at 600°/s, but is also subject to translation due to the movement of the cart. As a result, the angular rotation of the target varies between 380 and 1340°/s. Its linear speed component (in the horizontal plane) varies between 450 and 1060 mm/s with a mean of 700 mm/s. Along this trajectory, the target changes both direction and velocity, which makes it closer to the kinematics of the female flight. In our pilot study we focused only on capture chases, i.e. when the pursuer successfully catches the target in mid-air. Fig. 7 shows some of the results, in addition to the 3D reconstruction of one chasing flight in the experimental arena together with a top and side view of the entire sequence. This capture sequence occurs in about half a second. The chaser was hovering close to a wall oriented opposite to the target when he detected it.

The start of a pursuit is initiated when the fly detects the target. It is easily identified in the recorded image sequences as the pursuer

changes its body orientation in a saccade-like way followed by an acceleration phase. In Fig. 7C the position of the fly at the point in time before the body saccade is plotted relative to the target position. The data suggests that pursuit flights are initiated independently of the current position of the fly.

An important parameter for the analysis of the pursuit flight trajectory is the Distance To Target (DTT) presented in Fig. 7F. The change of this parameter can give valuable information about the strategy if it is not linear (Wardill et al., 2017; Kane et al., 2015). This change of this parameter along the *z*-axis (or altitude), which has rarely been taken into account in previous studies, is highly relevant when it comes to a 3D model of aerial pursuit strategies (see Fig. 7D and F). It is also required for estimating forces (here lift) the fly produces when approaching the target.

3.2. Parameters describing the orientation of the fly during pursuit flights

The knowledge of velocity vector during a flight trajectory alone does not necessarily allow us to reconstruct the region of the eyes onto which the image of a target is projected because its direction may not be aligned with body orientation of the animal in case of drift or sideslip (Wagner, 1986b). Thus, to characterize pursuit strategies, we will take care on analysing three lines and the angles they form with the reference frame.

The longitudinal body axis of the fly, here called Line of Body (LoB), defines the body orientation (see **OH** in Fig. 5E, θb Fig. 5E and Fig. 7G). Yaw and Pitch are the two angles that define this line. The Line of Sight (LoS), is the line connecting the centre of mass of the fly with the target (see **PT** in Fig. 5E, θa Fig. 5E and Fig. 7G), it is defined by the target bearing angle. The direction of travel, or Line of Flight (LoF) is defined by the line connecting the previous and the next positions in time of the fly. It is same as the tangential line of the flight trajectory, also referred to heading direction in literature.

It is important to note that in the context of aerial pursuit, the term “Error Angle” that is often found in the literature, may have different meanings. Here we propose the analysis of two error angles, defined by the three lines presented above. The error angle 1 (e1), is the angle formed by the LoS and the LoB. This angle characterizes the alignment of the body with the target position. In the case that the head is fixed to the body, it is directly linked to the position of the target on the fly's retina. The second parameter here called error angle 2 (e2), is the angle formed by the LoS and the LoF as defined by Land and Collett (1974). This angle gives information about the kinematics of the pursuit's strategy (Fajen and Warren, 2007; Gonzalez-Bellido et al., 2016).

In this account we define the orientation of the fly by its yaw-, pitch- and roll- angles. This means that in an absolute coordinate system, angles which are relative to the orientation of the fly will have an azimuth and an elevation component. The method proposed here allows us to separately extract and analyse those components along the entire pursuit flight sequence. The comparison between the two types of trajectories (circle and spinning top) suggest that the target speed does not affect the azimuth of error angle 1 (two samples t-test: $p(\theta e1) = 0.46$). The Line of the Body stays aligned to the Line of Sight, so the pursuer holds the target in the central part of its visual field, in the ‘love spot’ position.

In predatory species or in species where males catch female on the wing (Land and Nilsson, 2012), we observe a functional regionalization of the compound eye. In the former case, the animals are endowed with a small area in the frontal eye around the eye equator and above that features exceptionally high spatial resolution (van Hateren et al., 1989; Wardill et al., 2017; Sherk, 1978). Similar functional adaptation in the context of mating have been reported in various fly species including hoverflies and blowflies (Collett and Land, 1975; Land and Eckert, 1985), supported by high performance photoreceptors (Burton and Laughlin, 2003; Hornstein et al., 2000). In either case, only a specialized high resolution area of the eye provides sufficiently fast and robust visual input to support tightly controlled pursuit flights. This requires, as presented above, an orientation of the visual system where the target is projected onto this specialized region of the eye.

We measured the two error angles when presenting to the males the two trajectories described above. Regardless of the trajectories (and so to the angular velocity tested), the two errors are significantly different (two samples t-test: $p(\theta e1,\ \theta e2) = 9E\text{-}17$, $p(\varphi e1,\ \varphi e2) = 2E\text{-}97$) see Fig. 7H. This emphasizes the non alignment of LoS and LoB, causes are discussed below.

4. Discussion

We have developed a novel experimental setup that enables us to monitor the 3-dimensional movements of a freely flying fly chasing a dummy target along an arbitrary 2-dimensional trajectory. The quantitative analysis of the dummy movements shows that our method enables us to generate highly reproducible trajectories across tries. Both target position and the position of a pursuing fly are monitored and reconstructed at high spatial as well as temporal resolution, including the pursuer's body orientation. Those data are instrumental to retrieve the kinematics of the pursuing fly and to study the visual parameters the animal controls during chases.

A system adapted to blowfly and housefly speed. Our setup does not have the capability to generate dummy speeds equivalent to those of the hoverfly *Eristalis tenax* female, which, according to Collett and Land (1978), was assumed to reach maximum speeds up to 8 m/s. But it can generate maximum dummy velocities of 3 m/s which is adequate to study slower fly species such as blowflies and houseflies, where females fly at mean speeds of 1.2 and 0.65 m/s, respectively (Ennos, 1989; Land and Collett, 1974). A target velocity of 3 m/s was the maximum obtained when it was mounted on a 15 cm long rod (see Fig. 8B). Amongst Diptera, *Eristalis tenax* is considered the most agile, responding to a change of the target trajectory in as little as 20 ms. Other Dipteran pursuers have a longer reaction time. Male *Fannia*, for instance, respond only after 30 ms (Land and Collett, 1974). Time response of the chasing behaviour of *Lucilia* has not been measured yet. Boeddeker and Egelhaaf (2003), nonetheless, have implemented a model of *Lucilia* pursuing a target, that assumes a response delay of only 15 ms based on the analysis of the Line of Flight (LoF). Our flight trajectory acquisition system allows us to detect changes both in LoF and body orientation (LoB) with a temporal resolution limited by the 5.3 ms time interval between two consecutive frames. This acquisition speed is enough to check the values of the model created by Boeddeker and Egelhaaf (2003) which will be presented in an article in preparation.

The body orientation of the pursuer. In first experiments on *Lucilia* we focused on our hypothesis regarding the body orientation of the male fly during pursuit. When considering the pursuer as a ellipsoid body, defined by the position of its center of mass and two angles orientations: absolute yaw and pitch angles, we observed that the fly do not have the same orientation profile when chasing a dummy that executes slow or fast angular moves. We presented to the males two target trajectories, ‘circular’ and ‘spinning top’, that differ in target angular velocity (see Fig. 7 caption for trajectories’ details).

Horizontal plane: body yaw, heading, and side-slips. Over the range of target velocities we tested, flies always aligned their longitudinal body axis (yaw- orientation) with the line of sight (LoS) to keep the image of target projected onto their ‘love spot’. But we observed that the horizontal component of the LoF is hardly aligned with the LoS at high angular velocities (significant difference between the two angular velocities $p = 0.002$). This difference is likely the result of inertia-based side-slip during fast trajectory changes which, to our knowledge, has not been analysed during chasing flights before. Tested target trajectories included only clockwise rotation components. As a result, the values for the angle $\theta e2$ relative to LoS and LoF are always larger than those for $\theta e1$ relative to LoS and LoB (see Fig. 7H). This difference is probably the consequence of the animal's side-slip component which is

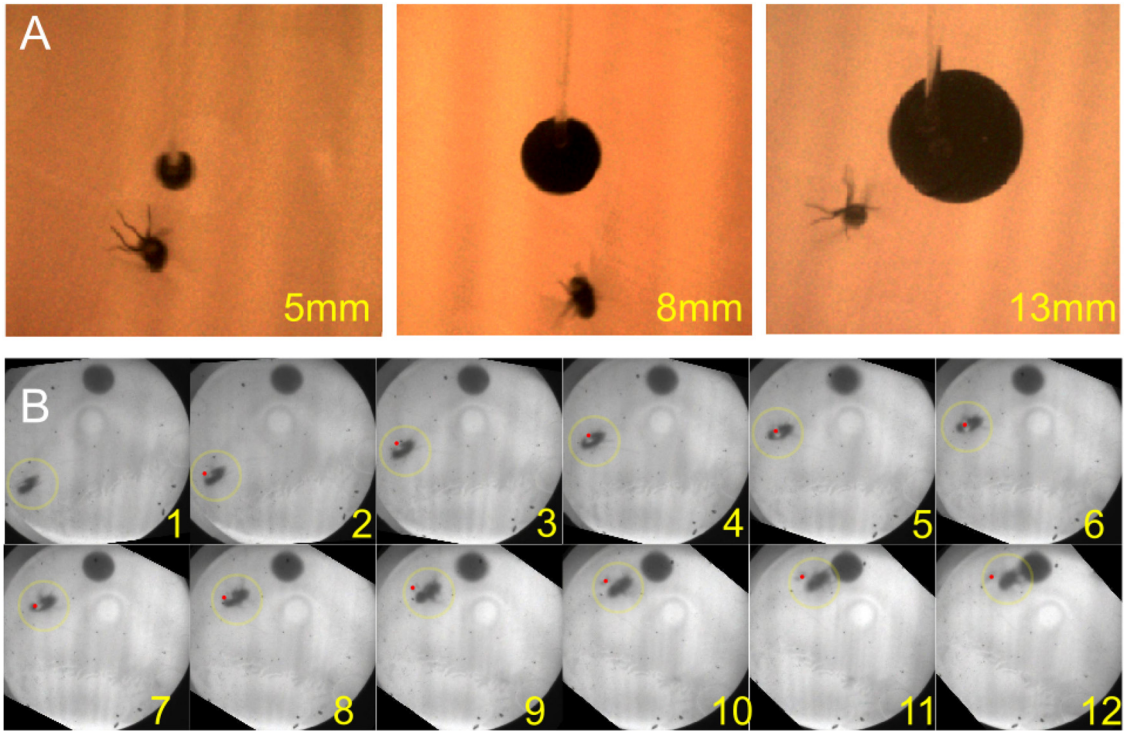

Fig. 8. Embedded pictures of the target and the pursuer. (A) Three pictures taken from the MicroCamera placed originally in the vertical tube of the moving cart (see Fig. 1C). Three sizes of targets have been tested to evaluate the field of view of the rotating mirror. The micro-endoscope module (MEM) allows us to detect the pursuer's legs, wings and eyes in the video footage. (B) Last 63 ms of the target capture presented in Fig. 7A, monitored with the MEM as described in Fig. 1C. The pursuer approaches the target before the final catch. A small flag was waxed onto the pursuer's dorsal thorax indicating its dorso-ventral body axis. Tracking the tip of the flag (red dot) enables the reconstruction of the external body roll- coordinate. Reconstruction of the full body attitude (yaw-, pitch- and roll-) is possible at high temporal resolution (5.3 ms).

always directed outwards with respect to its turning radius. Had we applied symmetrical clockwise and counter-clockwise rotation components to the dummy trajectories, we could have easily missed the difference as positive and negative values of $\theta e2$ would have cancelled out each other. To confirm our observation in future experiments we will generate dummy movements with symmetrical rotation components, e.g. 'figure-8-trajectories', analysing the un-signed angular data separately for clockwise and counter-clockwise rotation components.

Body pitch and the altitude changes. We did not observe significant differences $p = 0.09$ of the angle $\varphi e2$ (elevation angle formed between LoS and LoF) when target moved at slow or fast angular velocity. This suggests the absence of vertical-slips in the sagittal plane, in other words there is no inertia dependant offset in the x–z plane. To further investigation adjustment of the elevation component of the LoF, we would have to introduce changes in the z-position of the moving target, which should in principle be possible by means of slight alterations of our current setup.

Head-body fixation. Aerial pursuits in blowflies usually occur in less than 500 ms, from detection of the target to capture. During the chase, the male fly reaches maximum speeds of 2 m/s. Even at such high speed vision can provide the chaser fast and accurate information about the position of the target. Such challenging chasing flights have been modelled following two different approaches: kinematic models, and sensory-motor models. The large variety of target trajectories our new setup enables us to generate, will help to develop more general models of the pursuit, which include additional relevant parameters such as absolute and fly-centred orientation of the body, side-slips, and retinal position of the target. Initially, however, we will have to make an assumption that was made in previous modelling approaches, e.g. by Boeddeker et al. (2003): the head of the fly is aligned with and attached to the thorax, excluding any relative head-body movements. This constraint may be overcome once our micro-endoscope module (MEM) provides us with quantitative data on head-body rotations (see below). In the following we will discuss current modelling approaches on chasing flights.

Kinematic models of the chasing fly. They allow the analysis of capture strategies (Pal, 2015) as a balance between speed and manoeuvrability (Howland, 1974). They also characterize the pursuer's flight envelope. Once we designed the pursuer's object, here an ellipsoid defined by its centre of mass and its yaw- and pitch- angles, its envelop can be defined as the possible combination of translational and rotational movement components. Our method enables us to measure 3D target and pursuer positions with a maximum error of 5 mm. This position error is due to distortions caused by the camera optics, increased with increasing eccentricity and distance from the cameras, but less than 2 mm when the fly in the center of the arena. The chasing fly's yaw- and pitch- body orientation are measured with an error smaller than 6°, sampled every 5.3 ms. This makes the method suitable for building acceptable kinematic model of the pursuit. In comparison, the latest kinematic model of the blowfly pursuer (Boeddeker and Egelhaaf, 2003) was based on pursuits recorded in a cubic flight arena with 30 cm size, where the target moved along a circular path at constant speed. In this study, 3D-reconstruction system offered a spatial resolution of ± 1.5 mm and temporal resolution of 20 ms, which was same order of magnitude that the 15 ms delay to change the heading angle. In addition, body pitch- and roll- of the fly could not be extracted.

Banked turns in insect flights. Previous studies suggested that fruit flies are able to change their heading direction without banking by generating torque about their yaw- axis (Götz, 1964; Hedrick et al., 2009; Bergou et al., 2010). More recent studies, however, have shown that during fast escape manoeuvres they do perform banked turns (Muijres et al., 2014; Karasek et al., 2018). For a blowfly with a significant inertia operating at Reynolds number around 600 (Buckholz, 1981), banked turns are common during body saccade (Schilstra and

Hateren, 1999). Whether or not blowflies perform banked turns when engaging on chasing flights has not yet been systematically studied, but our first observations suggest that they do.

Body pitch, forward speed, and the changes of heading. We observed that the elevation coordinate of the error angle between LoS and LoB (see $\varphi e1$ in Fig. 7G) is significantly different ($p = 0.01$) when the target moves with slow or high angular velocity. This can be explained by a two steps relation. First, the linear relation between the forward speed and the absolute pitch- angle as described in blowfly by Schilstra and Hateren (1999), then if we consider the pursuer as a fixed-wing aircraft, the banking angle formula $\dot{\theta_p} = g/\mathrm{Va} \times \tan(\Omega)$ (Beard and McLain, 2012) gives us that the change of heading ($\dot{\theta_p}$) is linked to the forward speed (Va), with Ω the banking angle and g the gravitational field strength. This testify the relation we found between the absolute body pitch angle and the change of heading (linked itself to the angular velocity of the target), and so, the importance of banked turns in chasing.

To develop a realistic dynamic model of chasing flights taking into account the banked turns, the fly's body roll- component has to be included.

Banking angle and roll- angle. Nonetheless, banking angle or roll-angle has to be clarified. Assuming the flight kinematics of the a blowfly are similar to those of a fixed-wing aircraft, the most efficient way of changing flight direction would be the performance of coordinated turns (McClamroch, 2011) such as honeybees when loitering around the beehive (Mahadeeswara and Srinivasan, 2018). If xA, yA and zA are the axes of a fly- or aircraft-fixed coordinate system, the body roll- angle is defined as the rotation angle around xA (or the LoB axis). The banking angle is defined as the angle between the aircraft fixed yA and the horizontal plane, based on a rotation around the LoF. Thus, unlike the body roll- angle which is related to steady fly body orientation, the banking angle is linked to the fly's velocity vector. In coordinated flight, the side-slip angle is zero, so without a side-slip component the LoF is aligned with the LoB and the body roll- angle is equal to the banking angle. But in the presence of side-slips, the body roll- and banking angle are different. This will be taken into account when developing more general models of the pursuit (article in preparation).

Sensory-motor models. As mentioned earlier, an alternative to a kinematics-based model would be modelling the sensory-motor control loop of the fly during chasing flight. In the latter approach, visual information forms the sensory input to the system which is transformed into motor outputs controlling the fly's position and orientation. Gaze stabilization plays here a major role. To stabilize the visual input, in other words to keep the target in a fixed position of the retina, would be massively simplified with compensatory head roll (Hengstenberg, 1991; Hardcastle and Krapp, 2016). In the next paragraph we will present the additional module that will allow to quantify head-body rotations.

Close-up approach visualization module. Even more advanced real time video tracking systems such as the one developed by Straw et al. (2011) did not capture the roll orientation of the animal. Smaller arena can be an option, because of smaller distances and therefore higher spatial resolution in combination with focal depth of the cameras such as in Muijres et al. (2014), but it would be inadequate to study pursuit strategies in bigger species which require more space to perform chasing flights. Other techniques have been developed to estimate body roll during free cruising flight (Ristroph et al., 2009), in tethered flies (Tammero and Dickinson, 2002), or in semi-tethered flies (Schilstra and Van Hateren, 1998) but never during aerial pursuits in free flight. We have designed an addition functional module for our flight arena that will allow us to monitor the body orientation of the fly while chasing the target. We recorded chasing sequences using two configurations of this additional optical module (Fig. 1C).

The micro-camera and its low temporal resolution. Our video footage so far allowed us to identify the legs and some details of the approaching fly's head. The first version of this module consisted of a micro-camera (NanEye from Awaiba) facing a rotating mirror that keeps the target in the camera's field of view (Fig. 8A). Our first results validate the functional design of the module which enables us to stabilize a frontal view of the chasing fly even during a curved trajectory of the dummy. They also confirmed qualitative observation of banked turns during those pursuits, where the body roll- angle can assume values above 90°. The initial test version of the module, however, did not have sufficient temporal resolution to support a meaningful quantitative analysis of the video footage.

The micro-endoscope method (MEM). The second version of the module was based on a microendoscope technique, proposed by Pierce et al. (2011). This technique offers a high temporal resolution configuration that can be used to monitor the pursuer's body orientation until when the pursuer catches the dummy. We performed first tests using a 50,000 pixels optical fibre bundle (MyriadFiber) combined with a 1 mm Grin lens (infinity focal depth, and visual field of 60°, GrinTech). Images were transmitted via the optical fibre bundle to a CCD camera, which was equipped with a microscope objective focused on the end of the fibre bundle. The CCD camera was synchronized with the other 2 high speed cameras which monitored the position of the dummy and chasing fly at 190 fps. Fig. 8B shows the frames obtained during the final phase of a capture flight. A flag attached to the dorsal part of the thorax of the fly was tracked relative to the position of the legs to compute the roll angle of the fly. The spatial resolution with the 50,000 pixels fibre bundle was not high enough to extract confidently the body angle in all pursuits, but in the latest version we are implementing a 100,000 pixels fibre bundle which will give enough spatial resolution for further investigations.

Head-body rotations. Movements of the head relative to the body have minimum impact on the general trajectory of the fly when considering a kinematic model of the pursuit. However, as the movement of the head relative to the body significantly affects the retinal position of the target, it plays a major role when the pursuit is modelled from a sensory-motor perspective. The general assumption is that body roll is compensated by head rotations (Hardcastle and Krapp, 2016). This still needs experimental support in connection with chasing flights. The head of the fly in the video frame shown in Fig. 8A appears not to be in a horizontal orientation. Even if the gaze was stabilized around the roll axis, the fly might as well use head yaw and head pitch to keep the image of the target projected onto the love spot. Head's yaw- and pitch- also need to be assessed for similar reasons. The MEM module will enable us to monitor head orientation which will help us to analyse the visual parameters that flies control during chasing flights.

External perturbations. Chasing behaviour in flies occurs in many different natural environments such as bushes, empty fields, forests and even indoor below chandeliers (Land and Collett, 1974). The presented setup is a good support to investigate how the pursuit course is affected by external perturbations such as obstacles or wind.

Conflict of interest

None declared.

Author contribution

L.V.-P. designed the experimental setup and wrote the paper. H.G.-K. and S.V. provided administrative and scientific support, they verified the results and corrected the paper. S.V. proposed the principle based on a micro-camera and a rotating mirror to record the target point of view. All authors read and commented on the manuscript.

Acknowledgments

We would like to thank Julien Diperi, and Marc Boyron for their technical support. Roman Goulard, Ben Hardcastle and Jiaqi Huang for fruitful discussions. This work was supported by DGA through the co-supervised Fr UK PhD program. S.V. acknowledges support from the

Centre National de la Recherche Scientifique (CNRS), Aix-Marseille Universite and the Agence Nationale de la Recherche (ANR) [with the EVA project (Autonomous Flying Entomopter) and the IRIS project (Intelligent Retina for Innovative Sensing) ANR-12-INSE-0009].

Appendix A. Supplementary data

Supplementary data associated with this article can be found, in the online version, at https://doi.org/10.1016/j.jneumeth.2019.04.006.

References

Aziz, A., Karara, H., 1971. Direct linear transformation into object space coordinates in close-range photogrammetry. Proc. of the Symposium on Close-Range Photogrammetry 1–18.

Beard, R.W., McLain, T.W., 2012. "Small Unmanned Aircraft: Theory and Practice | Princeton University Press". Princeton University, The Trustees of Princeton University. press.princeton.edu/titles/9632.html.

Bergou, A.J., Ristroph, L., Guckenheimer, J., Cohen, I., Wang, Z.J., 2010. Fruit flies modulate passive wing pitching to generate in-flight turns. Phys. Rev. Lett. 104 (14). https://doi.org/10.1103/physrevlett.104.148101.

Boeddeker, N., Egelhaaf, M., 2003. Steering a virtual blowfly: simulation of visual pursuit, Proceedings. Proc. R. Soc. B: Biol. Sci. 270 (1527), 1971–1978.

Boeddeker, N., Kern, R., Egelhaaf, M., 2003. Chasing a dummy target: smooth pursuit and velocity control in male blowflies, Proceedings. Proc. R. Soc. B: Biol. Sci. 270 (1513), 393–399.

Buckholz, R.H., 1981. Measurements of unsteady periodic forces generated by the blowfly flying in a wind tunnel. J. Exp. Biol. 90, 163–173.

Burton, B.G., Laughlin, S.B., 2003. Neural images of pursuit targets in the photoreceptor arrays of male and female houseflies *Musca domestica*. J. Exp. Biol. 206 (22), 3963–3977.

Collett, T.S., Land, M.F., 1975. Visual control of flight behaviour in the hoverfly *Syritta pipiens* L. J. Compar. Physiol. A 99 (1), 1–66.

Collett, T.S., Land, M.F., 1978. How hoverflies compute interception courses. J. Compar. Physiol. A 125 (3), 191–204.

Egelhaaf, M., Borst, A., 1993. A look into the cockpit of the fly: visual orientation, algorithms, and identified neurons. J. Neurosci. 13 (11), 4563–4574.

Ennos, B.Y.A.R., 1989. The kinematics and aerodynamics of the free flight of some diptera. J. Exp. Biol. 85, 49–85.

Fajen, B.R., Warren, W.H., 2007. Behavioral dynamics of intercepting a moving target. Experimental Brain Research.

Gonzalez-Bellido, P.T., Fabian, S.T., Nordström, K., 2016. Target detection in insects: optical, neural and behavioral optimizations. Curr. Opin. Neurobiol. 41, 122–128.

Götz, K.G., 1964. 0ptomotorische Untersuchung des visuellen Systems einiger Augenmutanten der Fruehtfliege Drosophila. Kybernetik 2 (2), 77–92.

Hardcastle, B.J., Krapp, H.G., 2016. Evolution of biological image stabilization. Curr. Biol. 26 (20), R1010–R1021.

Harris, W.A., Stark, W.S., Walker, J.A., 1976. Genetic dissection of the photoreceptor system in the compound eye of *Drosophila melanogaster*. J. Physiol. 256, 415–439.

Hedrick, T.L., 2008. Software techniques for two- and three-dimensional kinematic measurements of biological and biomimetic systems. Bioinspir. Biomim. 3 (3), 034001.

Hedrick, T.L., Cheng, B., Deng, X., 2009. Wingbeat time and the scaling of passive rotational damping in flapping flight. Science 324 (5924), 252–255.

Hengstenberg, R., 1991. Gaze control in the blowfly Calliphora: a multisensory, two-stage integration process. Semin. Neurosci. 3 (1), 19–29.

Hornstein, E.P., O'Carroll, D.C., Anderson, J.C., Laughlin, S.B., 2000. Sexual dimorphism matches photoreceptor performance to behavioural requirements. Proc. R. Soc. B: Biol. Sci. 267 (1457), 2111–2117.

Howland, H.C., 1974. Optimal strategies for predator avoidance: the relative importance of speed and manoeuvrability. J. Theor. Biol. 47 (2), 333–350.

Mayer, I.E., 2012. corexy.com.

Kane, S.A., Fulton, A.H., Rosenthal, L.J., 2015. When hawks attack: animal-borne video studies of goshawk pursuit and prey-evasion strategies. J. Exp. Biol. 218 (Pt 2), 212–222.

Karasek, M., Muijres, F.T., Wagter, C.D., Remes, B.D.W., de Croon, G.C.H.E., 2018. A tailless aerial robotic flapper reveals that flies use torque coupling in rapid banked turns. Science 2 (September), 1089–1094.

Land, M.F., 1993. The visual control of courtship behaviour in the fly *Poecilobothrus nobilitatus*. J. Compar. Physiol. A 173 (5), 595–603.

Land, M.F., Collett, T.S., 1974. Chasing behaviour of houseflies (*Fannia canicularis*). J. Compar. Physiol. 89 (4), 331–357.

Land, M.F., Eckert, H., 1985. Maps of the acute zones of fly eyes. J. Compar. Physiol. A 156 (4), 525–538.

Land, M.F., Nilsson, D.-E., 2012. Animal Eyes, Volume 2.

Mahadeeswara, M.Y., Srinivasan, M.V., 2018. Coordinated Turning Behaviour of Loitering Honeybees. Sci. Rep. 8 (1), 1–14.

McClamroch, N.H., 2011. Steady Aircraft Flight and Performance. Princeton University Press.

Menzel, R., Backhaus, W., 1991. Colour vision in insects. In: Gouras, P. (Ed.), Vision and Visual Dysfunction. The Perception of Colour. MacMillan, London, pp. 262–288.

Mischiati, M., Lin, H.-T., Herold, P., Imler, E., Olberg, R., Leonardo, A., 2015. Internal models direct dragonfly interception steering. Nature 517 (7534), 333–338.

Muijres, F.T., Elzinga, M.J., Melis, J.M., Dickinson, M.H., 2014. Flies evade looming targets by executing rapid visually directed banked turns. Science 344 (4), 172–177.

Olberg, R.M., Seaman, R.C., Coats, M.I., Henry, A.F., 2007. Eye movements and target fixation during dragonfly prey-interception flights. J. Compar. Physiol. A: Neuroethol. Sensory Neural Behav. Physiol. 193 (7), 685–693.

Olberg, R.M., Worthington, A.H., Venator, K.R., 2000. Prey pursuit and interception in dragonflies. J. Compar. Physiol. A: Sensory Neural Behav. Physiol. 186 (2), 155–162.

Pal, S., 2015. Dynamics of aerial target pursuit. Eur. Phys. J. Spec. Top. 224 (17-18), 3295–3309.

Pierce, M., Yu, D., Richards-Kortum, R., 2011. High-resolution fiber-optic microendoscopy for in situ cellular imaging. J. Vis. Exp. 47, e2306.

Portelli, G., Ruffier, F., Franceschini, N., 2010. Honeybees change their height to restore their optic flow. J. Compar. Physiol. A: Neuroethol. Sensory Neural Behav. Physiol. 196 (4), 307–313.

Ristroph, L., Berman, G.J., Bergou, A.J., Wang, Z.J., Cohen, I., 2009. Automated hull reconstruction motion tracking (HRMT) applied to sideways maneuvers of free-flying insects. J. Exp. Biol. 212, 1324–1335.

Schilstra, C., Hateren, J., 1999. Blowfly flight and optic flow. I. Thorax kinematics and flight dynamics. J. Exp. Biol. 202 (11), 1481–1490.

Schilstra, C., Van Hateren, J.H., 1998. Using miniature sensor coils for simultaneous measurement of orientation and position of small, fast-moving animals. J. Neurosci. Methods 83 (2), 125–131.

Sherk, T.E., 1978. Development of the compound eyes of dragonflies (odonata). III. Adult compound eyes. J. Exp. Zool. 203 (1), 61–79.

Sollmann, K.S., Jouaneh, M.K., Lavender, D., 2010. Dynamic modeling of a two-axis, parallel, H-frame-type XY positioning system. IEEE/ASME Trans. Mechatron. 15 (2), 280–290.

Straw, A.D., Branson, K., Neumann, T.R., Dickinson, M.H., 2011. Multi-camera real-time three-dimensional tracking of multiple flying animals. J. R. Soc. Interface 8 (56), 395–409.

Tammero, L.F., Dickinson, M.H., 2002. Collision-avoidance and landing responses are mediated by separate pathways in the fruit fly, *Drosophila melanogaster*. J. Exp. Biol. 205 (Pt 18), 2785–2798.

van Hateren, J.H., Hardie, R.C., Rudolph, A., Laughlin, S.B., Stavenga, D.G., 1989. The bright zone, a specialized dorsal eye region in the male blowfly *Chrysomyia megacephala*. J. Compar. Physiol. A 164 (3), 297–308.

Wagner, H., 1986a. Flight performance and visual control of flight of the free-flying housefly (*Musca domestica* L.). II. Pursuit of targets. Proc. Trans. R. Soc. B: Biol. Sci. 312 (1158), 527–551.

Wagner, H., 1986b. Flight performance and visual control of flight of the free-flying housefly (*Musca Domestica* L.). III. Interactions between angular movement induced by wide- and smallfield stimuli. Proc. Trans. R. Soc. B: Biol. Sci. 312 (1158), 581–595.

Wardill, T.J., Fabian, S.T., Pettigrew, A.C., Stavenga, D.G., Nordström, K., Gonzalez-Bellido, P.T., 2017. A novel interception strategy in a miniature robber fly with extreme visual acuity. Curr. Biol. 27 (6), 854–859.

Wardill, T.J., Knowles, K., Barlow, L., Tapia, G., Nordström, K., Olberg, R.M., Gonzalez-Bellido, P.T., 2015. The killer fly hunger games: target size and speed predict decision to pursuit. Brain Behav. Evol. 86 (October), 28–37.

Wehrhahn, C., 1979. Sex-specific differences in the chasing behaviour of houseflies (Musca). Biol. Cybernet. 32 (4), 239–241.

Wehrhahn, C., Poggio, T., Bülthoff, H., 1982. Tracking and chasing in houseflies (Musca) – an analysis of 3-D flight trajectories. Biol. Cybernet. 45 (2), 123–130.

Zeil, J., 1986. The territorial flight of male houseflies (*Fannia canicularis* L.). Behav. Ecol. Sociobiol. 19 (3), 213–219.